Atmos. Meas. Tech. Discuss., 7, 12407–12447, 2014
www.atmos-meas-tech-discuss.net/7/12407/2014/
doi:10.5194/amtd-7-12407-2014

Atmospheric Measurement Techniques Discussions
Open Access

Ceilometer aerosol profiling vs. Raman lidar in the frame of INTERACT campaign of ACTRIS

F. Madonna[1], **F. Amato**[1], **J. Vande Hey**[2], **and G. Pappalardo**[1]

[1]Consiglio Nazionale delle Ricerche, Istituto di Metodologie per l'Analisi Ambientale (CNR-IMAA), C.da S. Loja – Zona Industriale, 85050 Tito Scalo, Potenza, Italy
[2]University of Leicester, Department of Physics and Astronomy, Earth Observation Science Group, University Road, Leicester, LE1 7RH, UK

Received: 16 October 2014 – Accepted: 18 November 2014 – Published: 12 December 2014

Correspondence to: F. Madonna (fabio.madonna@imaa.cnr.it)

Published by Copernicus Publications on behalf of the European Geosciences Union.

Abstract

Despite their differences from more advanced and more powerful lidars, the low construction and operation cost of ceilometers, originally designed for cloud base height monitoring, has fostered their use for the quantitative study of aerosol properties. The large number of ceilometers available worldwide represents a strong motivation to investigate both the extent to which they can be used to fill in the geographical gaps between advanced lidar stations and also how their continuous data flow can be linked to existing networks of the more advanced lidars, like EARLINET (European Aerosol Research LIdar NETwork).

In this paper, multi-wavelength Raman lidar measurements are used to investigate the capability of ceilometers to provide reliable information about atmospheric aerosol content through the INTERACT (INTERcomparison of Aerosol and Cloud Tracking) campaign carried out at the CNR-IMAA Atmospheric Observatory (760 m a.s.l., 40.60° N, 15.72° E), in the framework of ACTRIS (Aerosol Clouds Trace gases Research InfraStructure) FP7 project. This work is the first time that three different commercial ceilometers with an advanced Raman lidar are compared over a period of six months. The comparison of the attenuated backscatter profiles from a multi-wavelength Raman lidar and three ceilometers (CHM15k, CS135s, CT25K) reveals differences due to the expected discrepancy in the SNR but also due to effect of changes in the ambient temperature on the short and mid-term stability of ceilometer calibration. A large instability of ceilometers in the incomplete overlap region has also been observed, making the use of a single overlap correction function for the whole duration of the campaign critical. Therefore, technological improvements of ceilometers towards their operational use in the monitoring of the atmospheric aerosol in the low and free troposphere are needed.

AMTD
7, 12407–12447, 2014

1 Introduction

For the study of climate as well as that of air pollution and its influence on health, knowledge of vertical distributions of aerosols is a key factor. From the climate point of view, the aerosol vertical layering is required for the study of aerosol radiative forcing, aerosol-cloud interactions, and aerosol transport mechanisms. For air pollution and its impact on health, it is essential to know the concentrations and properties of aerosols located near the surface in near-real time in order to understand population exposure. This scenario has pushed the demand for continuous aerosol measurements provided by high resolution networks of ground-based instruments to validate and improve aerosol and pollution forecasting. In order to achieve broad, high resolution coverage, low-cost and low-maintenance instruments are needed.

Ceilometers are inexpensive instruments whose cost is typically in the EUR 12 000–20 000 range, except for a couple of models closer to EUR 45 000. Ceilometers are already deployed widely at meteorological observation stations and airports. Ceilometers are defined as single-wavelength backscatter lidars operating in the near-infrared with a pulse repetition rate on the order of a few kHz but with a low pulse energy to allow eye safe operation. These instruments are based on the lidar principle and measure elastically-backscattered returns, usually at 905–910 or 1064 nm, and have traditionally been used only to report cloud base and vertical visibility rather than the vertical profiles of the aerosol backscatter coefficient on which they are basing these outputs. They have been also used to evaluate the cloud fraction as provided by mesoscale models (Illingworth et al., 2007). In recent years, due to their technical advances, ceilometers show great potential for aerosol applications such as volcanic ash tracking (e.g. Flentje et al., 2010; Emeis et al., 2011; Wiegner et al., 2012) and boundary layer monitoring (e.g. Tsaknakis et al., 2011).

The large number of ceilometers available worldwide (cfr. http://www.dwd.de/ceilomap) represents a strong motivation to investigate the extent to which they can be used to fill the geographical gaps between advanced lidar stations within existing

AMTD
7, 12407–12447, 2014

networks like EARLINET (European Aerosol research LIdar NETwork) and also how their continuous data flow can be linked to these networks. To fully exploit this observing capability, the E-PROFILE (http://www.eumetnet.eu/e-profile) observation program, run by the European Met Services, is developing a framework to exchange lidar backscatter data from automatic lidars and ceilometers stations across Europe.

To retrieve the vertical profile of aerosol optical properties from a ceilometer, several approaches have been proposed (e.g. O'Connor et al., 2004; Markowicz et al., 2008; Heese at al. 2010; Flentje et al., 2010; Stachlewska et al., 2010; Wiegner et al., 2012) either based on the use of ceilometer measurement only or in combination with ancillary measurements provided by a sun photometer or a nephelometer.

However, thorough characterization of ceilometer sensitivity, stability, bias and uncertainty for the observation of aerosol layers is missing and needed in order to develop the rigorous quality assurance program that will enable full exploitation of the ceilometer data.

In this paper, the outcome of the INTERACT campaign, funded and carried out in the frame of the ACTRIS (Aerosol Clouds Trace gases Research InfraStructure – www.actris.org) transnational access activities is described. The campaign was held at CIAO, CNR-IMAA Atmospheric Observatory (760 m a.s.l., 40.60° N, 15.72° E) in the period from July 2013 to January 2014 with the aim to improve understanding of ceilometer performance. This work represents the first time that three different commercial ceilometers are compared with an advanced Raman lidar over a period of six months. To this purpose multi-wavelength Raman lidar measurements are used to investigate the capability of ceilometers to provide reliable information about atmospheric aerosol content. The dataset used for this study has been collected at the observatory (Madonna et al., 2011), where MUSA (Multiwavelength System for Aerosol), one of the mobile reference systems used in the frame of the EARLINET Quality Assurance Program, is operative. 1064 nm MUSA attenuated backscatter profiles are compared with those provided by a CHM15k Jenoptik ceilometer operating at 1064 nm up to 15 km above the ground level (a.g.l.), run at CIAO since September 2009, by a VAISALA

AMTD
7, 12407–12447, 2014

CT25K ceilometer operating at 905 nm up to 7.5 km a.g.l., run at CIAO since 2005, and by a CS135s Campbell ceilometer prototype operating at 905 nm up to 10 km a.g.l., deployed at CIAO during INTERACT, provided by the manufacturer itself. Using the MUSA data products as the reference, the capability of ceilometers to detect aerosol layers and provide quantitative information about the atmospheric aerosol load is investigated.

In the next section, an overview of the INTERACT campaign, the instruments deployed during the period of the campaign, and the algorithms used for the data processing is provided. In Sect. 3, the stability of the ceilometers is discussed in comparison with the stability of the MUSA lidar. In Sect. 4, simultaneous ceilometer and lidar attenuated backscatter observations are evaluated. Summary and conclusions are finally reported in Sect. 5.

2 INTERACT campaign

2.1 Scientific objectives

The INTERACT campaign was held at CIAO in Potenza, Italy from 1 July 2013 to 12 January 2014, with the main scientific objective to evaluate the stability, sensitivity, and uncertainties of ceilometer aerosol backscatter profiles and the idiosyncrasies of ceilometer automated cloud base detection. Here, three commercial ceilometers from different manufactures are compared with an advanced multi-wavelength Raman lidar, and their aerosol detection sensitivity and stability are assessed using a dataset collected over a period of more than six months.

CIAO represents an ideal location for observations of maritime, continental and mineral aerosols observed under different weather regimes. Equally important, the observatory is equipped with further instruments, including two advanced lidar systems, two ceilometers (CHM15k by Jenoptik and CT25K by VAISALA), a microwave radiometer, a Ka-band radar, and an automated radiosonde launching system (Madonna et al.,

AMTD
7, 12407–12447, 2014

2011). With the addition of the third ceilometer delivered to the observatory by Campbell Scientific for the campaign, CIAO had a unique opportunity to carry out an intercomparison among Raman lidar and ceilometers.

2.2 Instruments

MUSA is a mobile multi-wavelength lidar system based on a Nd:YAG laser equipped with second and third harmonic generators and a Cassegrain telescope with a primary mirror of 300 mm diameter. The three laser beams at 1064, 532 and 355 nm are simultaneously and coaxially transmitted into the atmosphere beside the receiver in biaxial configuration. The receiving system has 3 channels for the detection of radiation elastically backscattered from the atmosphere and 2 channels for the detection of the Raman radiation backscattered by atmospheric N_2 molecules at 607 and 387 nm. The elastic channel at 532 nm is split into parallel and perpendicular polarization components by means of a polarizing beam splitter cube. The backscattered radiation at all the wavelengths is acquired by photomultiplier tubes both in analog and photon counting mode. The calibration of depolarization channels is made automatically using the ±45 method (Freudenthaler et al., 2009). The typical vertical resolution of the raw profiles is 3.75 m with a temporal resolution of 1 min.

The system is compact and transportable. It was developed in 2009 in cooperation with the Meteorological Institute of the Ludwig-Maximilians-Universität of Munich and it is one of the reference systems used for the EARLINET quality assurance program (Pappalardo et al., 2014).

Ceilometers are optical instruments based on the lidar principle but eye-safe and generally lower in cost than advanced research lidars. Their primary application is the determination of cloud base height, but they are also expected to report vertical visibility for transport-related meteorology applications. Increasingly they are expected to output attenuated backscatter profiles as well (e.g. Wiegner and Geiß, 2012) and are being trialed for aerosol mixing layer height measurement for air quality applications (e.g. Cimini et al., 2013). These instruments typically have signal to noise ratios

AMTD
7, 12407–12447, 2014

(SNRs) considerably lower than lidar systems because of wider optical bandpass filters required to accommodate broader spectrum inexpensive diode laser sources. Eye safety restrictions on laser power output also affect the SNR. Two of the ceilometers used in this study, the CT25k and the CS135s, are based on diode lasers while the third, the Jenoptik CHM15k, is based on narrower linewidth solid state laser technology (Nd:YAG diode-pumped laser). Compared to most of the lidar systems, ceilometers have the important advantage of being designed to be deployed unattended in the field for many years with minimal maintenance. Further information on how to discriminate a lidar, basic or advanced, from a ceilometer is provided in Wiegner et al. (2014).

Ceilometers also have several drawbacks. First of all, not all of them provide the raw backscattered signals and their processing software tends to be a sort of "black box" for users. Moreover, ceilometer hardware can be accessed by the user and also partly tested for maintenance purposes but auto-adjustments of the hardware settings performed by the manufacturers' software typically gives little or no control to the user. Ceilometer gain (or sensitivity) changes automatically depending upon backscatter and background light levels, for example from daytime to nighttime measurements or in the presence of scattered clouds. The instrument's gain can be suddenly modified by a change in the high voltage supply of the detector (an avalanche photodiode – APD) and, therefore, the gain level is factored into the raw signal or the attenuated backscatter calculation independently for each measurement. Nevertheless, it is quite difficult to characterize different ceilometers using one parameter, such as the gain, since this might be managed in very different ways among the different types of ceilometers. Therefore, more detailed studies on the dependence of the main products delivered by a ceilometer (raw signal or attenuated backscatter) are needed.

Table 1 reports the specifications of the ceilometers used during the INTERACT campaign along with those of MUSA.

The Jenoptik CHM15k is a biaxial ceilometer based on a 1064 nm Nd:YAG laser and a photon counting avalanche photodiode (APD); the instrument has a specified range of 15 km and full overlap at around 1500 m (Heese et al., 2010). Overlap correction

AMTD
7, 12407–12447, 2014

functions are provided by the manufacturer down to approximately 500 m. Automatic gain adjustments typically affecting Jenoptik ceilometers (Wiegner et al., 2014) are accounted for in this work and discussed later in the paper.

The Vaisala CT25K is a coaxial, common optics ceilometer based on a 905 nm diode laser and an analog silicon APD with a specified range of 7.5 km (Vaisala, 1999). The common optics configuration allows for close range onset of overlap according to the manual (Vaisala, 1999). The measurement range of the instrument is 0 to 25 000 ft or 7.5 km, which could imply that overlap onset occurs at 0. However this range most likely refers to sensitivity to clouds which can be detected through multiple scattering at close ranges although it also requires additional complexity in the form of a second APD which is needed to mitigate optical cross-talk (Markowicz et al., 2008). The instrument is well established as a tool for cloud base height measurement. Attenuated backscatter profiles are produced automatically from raw signals not available from the instrument and the internal corrections and filtering are not specified.

The Campbell Scientific CS135s is a pre-production prototype of the recently released CS135 ceilometer. Like the CT25k, the instrument employs a 905 nm diode laser and an analog-mode silicon APD. However, this instrument is based on a divided-lens biaxial design described in Vande Hey et al. (2012). The CS135 has a range of 10 km (Campbell Scientific, 2014). Currently overlap is corrected by application of a theoretical geometric optics overlap function which has been validated by horizontal hard target measurements (see Vande Hey et al., 2011). Single-scattering overlap onset is calculated to start at 75 m, though the instrument is sensitive to clouds from 10 m altitude range because of multiple scattering. Full overlap is reached at between about 300 and 400 m.

Geometric overlap corrections for any lidar instrument become unstable as overlap approaches zero; for the INTERACT campaign no data were evaluated below the full overlap range of MUSA which is at 405 m, therefore no overlap correction was applied to the CS135s data. “Raw” attenuated backscatter profiles were output from the CS135s. Unfortunately, the CS135s prototype suffered from an electronic distortion

AMTD
7, 12407–12447, 2014

that affected the data. Nevertheless, the calibration of CS135s was feasible and, except for the presence of a high noise level above 3000 m a.g.l., data can be compared and evaluated using MUSA data, as discussed later on in the paper.

2.3 Data processing

This section provides an overview of the processing algorithm used to compare MUSA and ceilometer observations. MUSA data (aerosol extinction and backscatter coefficients) are processed using the automatic Single Calculus Chain (SCC) of EARLINET (Pappalardo et al., 2014; D'Amico et al., 2014). The SCC is able to pre-process lidar signals to provide aerosol optical and geometrical properties (e.g. layering) using Raman and elastic algorithms (Ansmann et al., 1992).

CHM15k data are collected using the JO-Dataclient software provided by the manufacturer, while the attenuated backscatter profiles are obtained by normalizing the ceilometer range-corrected signals to the corresponding MUSA attenuated backscatter profiles. Normalization was first attempted using a region 1–2 km wide, located 6–7 km a.g.l. and identified as an aerosol free region identified from the quicklooks of the lidar measurements time series. This choice, however, tended to underestimate the normalization constant because of the very poor SNR of the ceilometer at those altitude levels. Throughout the campaign the ceilometer proved to be able to detect values of the attenuated backscatter larger than $1.0 \times 10^{-7}\,\mathrm{m^{-1}\,sr^{-1}}$ at altitude levels lower than 4 km a.g.l. with a vertical resolution of 30 m and a time resolution ranging from 45 to 120 min. Therefore, the normalization has been performed over a vertical range of 1 km, below the altitude level where this threshold value is detected. This typically occurs around 4 km. A detailed inspection of the normalization for each pair of MUSA and CHM15k profiles has been also performed to ensure the high quality of the normalization procedure.

CS135s raw signals have been collected using a terminal emulator; attenuated backscatter profiles are obtained upon normalization to the corresponding MUSA attenuated backscatter profiles using the same procedure followed for the CHM15k. Since

AMTD
7, 12407–12447, 2014

signals in the upper troposphere were affected by electronic distortion, the normalization region selected was typically immediately below 2.0–2.5 km in order to have a sufficient SNR to obtain a stable normalization over the lidar profiles.

The CT25K does not provide any raw signal besides the so-called normalized sensitivity backscatter coefficient output by the manufacturer's software; therefore, attenuated backscatter profiles can only be obtained using the cloud calibration technique (O'Connor et al., 2004). It is worth emphasizing that even though established calibration methods applied to the outputs of manufactures' software have been shown to be robust for cloud studies (e.g. O' Connor et al., 2004), it is nonetheless highly desirable to make available raw signals from all ceilometers. This is the only way to allow users to independently manage the whole data processing chain, to estimate the correction factors applied to the signals, and to quantify the total uncertainty budget.

All the ceilometers' attenuated backscatter profiles were compared with the lidar over a vertical resolution of 30 m and a time resolution ranging from 45 to 120 min. Time and vertical resolution were selected to keep the ceilometer SNR to sufficient levels to allow comparison to and calibration by MUSA. Only night time measurements were considered in this analysis in order to capture the best ceilometer performances and to allow the use of the roto-vibrational Raman signal. An extension of the current analysis to daytime is foreseen though this will make the use of a few assumptions on the MUSA retrieval mandatory (e.g. a fixed value of lidar ratio). In addition, for the CHM15k (to avoid problems with the sudden change of the calibration factor automatically selected by the ceilometer itself) only signals corresponding to a value of the "base" (daylight correction factor) parameter less than 0.0015 (low background light level) were considered. The use of relative calibration (Wiegner and Geiß, 2012) can also eliminate this problem during the whole day.

AMTD
7, 12407–12447, 2014

3 Instrumental stability

Ceilometer calibration is a crucial point for quantitative use of ceilometer data. Indeed the use of the Rayleigh calibration technique, based on the normalization of raw ceilometer signals (if available) on a molecular profile, is often challenging (Binietoglou et al., 2011; Wiegner et al., 2014). Moreover, when raw ceilometer signal are not available, the use of the outputs of manufacturer software can provide large discrepancies with respect to advanced or elastic lidar profiles. Therefore, the calibration of the ceilometer profile is often mandatory.

Calibration by means of forward approaches based on co-located and coincident reference measurements is one solution to allow quantitative use of ceilometer observations; periodic re-calibration from a Raman lidar or a high-spectral resolution lidar would be strongly suggested for long term calibrated use. However, the stability of the ceilometer in the periods between two calibrations needs to be checked. This type of investigation is limited if the manufacturer provides several parameters monitoring the activity of the instruments but does not provide full access to the raw signals and the processing chain.

During the INTERACT campaign, two of the ceilometers, CHM15k and CS135s prototype, provided full access to the instrument information. For both of them, the forward approach has been used and the stability of the calibration constant (CC) has been studied in correlation with the ceilometers' parameters, while for the CT25K the cloud calibration has been applied. CC is defined as:

$$\mathrm{CC} = \frac{P_{\mathrm{ceilo}} z^2}{\beta'_{\mathrm{MUSA}}} \tag{1}$$

where β'_{MUSA} is the attenuated backscatter obtained by MUSA, discussed in Sect. 5, P_{ceilo} is the ceilometer raw signal and z is the altitude.

Finally, to avoid effects that any, even small but possibly relevant, misalignment of the MUSA lidar could have on the comparison, all the plots reported in this section includ-

AMTD
7, 12407–12447, 2014

ing the MUSA attenuated backscatter were compared with the same plots obtained excluding all the data below 1000 m a.g.l. This height level is the typical level below which misalignments would more likely affect the MUSA signals than above. The outcome of the comparison is that no relevant differences are observed in the relationship between MUSA attenuated backscatter and ceilometer attenuated backscatter if all the values measured below 1 km a.g.l. are excluded.

3.1 CHM15k stability

In the left panel of Fig. 2, for the cases selected according to the criteria described in Sects. 2 and 3, CC has been plotted along with the lidar calibration constant (CL) used for the molecular retrieval of the 1064 nm lidar backscatter coefficient, i.e. the constant used to normalize the 1064 nm lidar profile over the molecular profile. CL is defined as:

$$\mathrm{CL} = \frac{P_{\mathrm{L}}}{\beta T^2}, \tag{2}$$

where P_{L} is the background-subtracted lidar signal, β is the total backscatter coefficient including molecules and particles, and T^2 is the atmospheric transmissivity.

Analysis of CL variability allows the stability of the lidar system to be tracked. The comparison shows that the variability of CC is quite high, 58 %, while the variability of CL is 15 %. Typically, CL is stable within 5–10 % but for the selected period MUSA was moved for an intercomparison campaign in South Italy (Wandinger et al., 2014), and then the configuration underwent the realignment procedure (after case number 16). Despite the changes in MUSA, the large variability of the CC cannot be fully attributed to the variability of MUSA. To better understand the large variability of CC, all the system parameters recorded for each ceilometer profile have been considered. For example, in the right panel of Fig. 2, the temperature of the ceilometer detector and the external (ambient) and internal temperatures of the instrument are reported. The reported ambient temperature has been compared also with a co-located surface measurement of temperature obtained with a Rotronic S3 sonde. The comparison

AMTD
7, 12407–12447, 2014

for the considered period shows the same temperature trend and a general agreement between the Rotronic sonde and the ceilometer temperature sensor within 1 K. The behavior of the internal temperature of the ceilometer looks quite well correlated with CC. The internal temperature is also well correlated with the ambient temperature. Indeed the correlation coefficient derived from a linear fitting between the ambient temperature and CC is 0.6. This could indicate that there is a not negligible influence of the internal temperature on the instrument stability over short and mid-periods (~ 6 months) likely driven by changes in the external temperature (i.e. change of season). This indicates that thermal insulation or, more generally, the capability to have stable thermal working conditions for the ceilometer experimental setup is critical. As a consequence, at the current state of the art, the use of a forward approach to calibrate a ceilometer using lidar observations cannot be reliable over long time periods. Calibration should be frequently checked and carefully evaluated. It is also worth adding that from personal communication (by M. Wiegner, LMU, Munich, Germany), this could also be related to the unreliability in the long term of the temperature sensors of the ceilometers which may use these temperature measurements to control system or component temperature or apply corrections, though it appears unlikely that this happened for all three deployed ceilometer systems, one of which (CS135s) was completely new and another (CHM15k) had a completely new optical module.

Correlation with the other available system parameters such as number of laser pulses or state of the laser have been also investigated but nothing relevant has been found. Moreover, the correlation between MUSA and CHM15k attenuated backscatter has been not studied because the CHM15k is calibrated over MUSA.

3.2 CT25k stability

Though limited by the lack of access to raw data, an attempt has been made to characterize the stability of CT25K. In Fig. 3, the laser temperature, the background light (though during night no significant changes are expected) and the receiver sensitivity as measured by the internal sensors of the CT25K ceilometer are reported for the

AMTD
7, 12407–12447, 2014

cases available for the comparison with MUSA. Around case number 25 (2 September 2014), it is possible to detect a decrease in all the parameters with respect to the corresponding average values. This corresponds to the period when the decrease of the CHM15k parameters discussed in the previous section took place, and more generally to the arrival of colder air masses over Potenza after the typical hot summertime in Southern Italy. Moreover, it is also worth noting the strong correlation between the laser temperature and the background light: since we are dealing with night time observations, this could indicate that most of the noise, due to the ceilometer electronics, is provided by the laser.

In the left panel of Fig. 4, the scatter plot of the attenuated backscatter retrieved by the ceilometer CT25K observations vs. the attenuated backscatter retrieved by MUSA observations is reported; in the right panel, only the measurements performed on or after 2 September 2013 are included. The correlation coefficient for the full data set is 0.78, but this increases to 0.94 if only the cases starting from 2 September 2013 are considered. Moreover, the left panel of Fig. 4 shows an intercept of 1.67×10^{-7} m^{-1} sr^{-1} indicating the presence of a bias at least partly affecting the dataset; the bias looks strongly reduced in the right panel.

This could indicate that the retrieval of the attenuated backscatter and, in general, ceilometer measurements strongly depend on the effect of the change of season on the investigated parameters whose decrease in the mentioned period is probably related to the decrease in ambient temperature. For the CT25k, these results again indicate that ceilometer stability even over periods of weeks to months cannot be ensured and therefore calibration constants calculated using the cloud calibration method (the standard approach for diode-based ceilometers) should be frequently checked and re-evaluated, probably on the scale of months.

The effect of water vapor on the stability of CC over time has also been evaluated. This effect is strongly related to the presence of a water vapor absorption band at 905–910 nm, while the effect of water vapor is limited at 1064 nm. This effect is considered in detail in Wiegner et al. (2014), where the relative error affecting CC is estimated to

AMTD
7, 12407–12447, 2014

be on the order of less than 20 %. In this work, the correlation between the variability of the calibration constant and the variability of the Integrated Water Vapor (IWV) content over time has been evaluated and reported in Fig. 5. The IWV is measured by GPS receiver operational at CIAO, and the processing of CIAO GPS data is provided by the NOAA/GSD Ground-Based GPS Meteorology network. During INTERACT the time series of the IWV shows values larger than 1.0 cm from 1 July 2013 to 10 October 2013 with values oscillating around about 2.0 cm. After 10 October 2013, a decrease in the IVW is observed with values oscillating around 1.25 cm and dipping below 1.0 cm. Since CC shows a relevant change after 2 September 2013, it is possible to conclude that the effect of water vapour on the value of CC needs to taken into account but it cannot entirely justify the variability of CC observed during INTERACT.

Also for the CT25K, correlation with the other available system parameters was investigated but nothing relevant was found.

3.3 CS135s stability

In analogy with the investigation presented in Sect. 3.1 for the CHM15k, in Fig. 6 CC has been plotted for the CS135s. The comparison shows that the variability of CC is quite high, larger than 100 % with a mean value of 3.25 and a SD of 3.76. For the CS135s, CC looks less affected than the other ceilometers by the change of season in the environmental temperature. Nevertheless, in the period after 3 October 2013 (case number 23) the value of CC becomes much more unstable with peak values around 17.31, largely different from the average value of the whole series. Also in this case, though there is not a specific correlation between CC and the internal or external temperature, as for the other ceilometers, calibration might depend on the environmental temperature. Moreover, the variability of CC for the CS135s is much larger than for the CHM15k. This cannot be related to the distortion affecting the signals but is likely due to the general stability of the CS135s over the campaign.

Moreover, for the CS135s, the period when the values of CC become much more unstable occurs in the same period when a seasonal decrease is observed in the IWV,

AMTD
7, 12407–12447, 2014

reported in Fig. 5. However, there is not a strong correlation with the value of CC and this might indicate that water vapor level is only one of the effects driving the variability of CC.

Correlation with the other available system parameters was also studied for CS135s but nothing relevant was found.

3.4 Overlap stability

Quantitative measurements of boundary layer aerosols in the near-field region using ceilometers also depend on the stability of the overlap factor with the time, on the accuracy of correction functions to be applied to ceilometer signals in the incomplete overlap region, and on the reliability of the near-field measurements used to establish the correction functions. As clarified in Wiegner et al. (2014), for the retrieval of aerosol properties incomplete overlap is not a severe issue. At typical ceilometer wavelengths and correction functions, incomplete overlap generally contributes a few percent of the uncertainty in the full overlap region. Nevertheless, overlap corrections should be applied, if available, in order to extend the investigated range closer to the instrument and improve layer retrieval closer to the surface. In order to properly characterize ceilometer (and lidar) measurement uncertainties, overlap corrections with associated confidence levels should be applied and the stability of these corrections should be tracked over time.

Typical overlap corrections range between 200–300 and 1000 m among different ceilometer types. To perform an independent evaluation of the stability of the instrument in the region of incomplete overlap, an analysis of the variability of the ratio $\frac{\beta'_{\mathrm{CEILO}}}{\beta'_{\mathrm{MUSA}}}$ between the attenuated backscatter measured by each ceilometer and by MUSA has been studied. Figure 7 shows the average (dark line) and SD (vertical bar) of the ratio between the attenuated backscatter measured by each ceilometer and MUSA. Altitude ranges above the first available point from MUSA in the full overlap region (405 m a.g.l.) have been considered. Since for the CHM15k, the Jenoptik overlap correction func-

AMTD
7, 12407–12447, 2014

tion covers altitudes starting from approximately 500 m a.g.l., the comparison covers a range appropriate for evaluating that ceilometer's performance in the near-field.

In the upper panel of Fig. 7, the comparison reveals a large variability in the region from 405 to 890 m a.g.l. Above 890 m a.g.l. the variability decreases, but the average ratio between CHM15k and MUSA decreases from a value of 1.8 at 405 m a.g.l. to 1.0 at 1000 m a.g.l., while above it continues to decrease until 1375 m a.g.l. when it becomes nearly constant; the variability remains larger than 50 %. This indicates instability of CHM15k in the incomplete overlap region. The effect of the overlap correction on the retrieval of aerosol backscatter coefficient (beyond the full overlap range) if using a forward approach can be easily quantified. However, it is clear that particular care should be taken in using a single overlap correction function, and its variability with time should be monitored. It is also important to point out that in the CHM15kx ceilometer this issue has been improved by tilting the axis of the laser toward the axis of the telescope. All the CHM15k data considered in the following to study the performance of the ceilometer in terms of attenuated backscatter were selected from 1300 m a.g.l. and above, in order to avoid uncertainties relating to overlap instability.

As described previously the CS135s is corrected automatically through the application of a calculated geometric optics overlap function (Vande Hey et al., 2011) which places the full overlap height between 300 and 400 m. The middle panel of Fig. 7 shows that the ratio between CS135s and MUSA remains largely between 0.5 and 0.6 from 405 to 1400 m a.g.l., suggesting relatively stable overlap in this region. Above this height the variability of the ratio between CS135s and MUSA is affected by differences in the attenuated backscatter calibration. It shows a variability even larger than 100 % at higher altitude levels affected by the discussed distortion in the CS135s signals, so it is not possible to see from these data whether the overlap remains stable.

In the case of CT25K the output profiles are already corrected for incomplete overlap, but the function itself is unknown to the user. As shown in Table 1, the laser divergence is greater than the field of view of the instrument, so full overlap is never reached. Using a geometric optics approach similar to that described in Vande Hey et al. (2011),

AMTD
7, 12407–12447, 2014

the parameters in the CT25K manual (VAISALA, 1999) can be used to calculate the optical overlap function of the instrument. By this method overlap is found to be 45 % at 100 m, 78 % at 300 m, and 85 % at 500 m, and it reaches maximum of 90 % at approximately 1000 m. Markowicz et al. (2008) reported observing overlap effects of the CT25k directly from its signal to up to 450–550 m, starting from which point the slope of the calculated overlap function is very small. However, since the internal corrections applied in the instrument are not known, the effective overlap of the instrument can only be understood through experimental comparisons with reference instruments or horizontal measurements under stable conditions. Note that the newer VAISALA CL31 ceilometer (not available at CIAO) is described with a considerably smaller overlap region than the CT25K. However, CT25K is still one of the most widely used ceilometers in Europe and this make the investigation of its performances relevant for the scientific community.

The lower panel of Fig. 7 reveals the higher stability of the CT25K with respect to the CHM15k and CS135s, even if the overlap function of the CT25K is not known. Nevertheless, the attenuated backscatter differs considerably from that of MUSA, which explains the deviation of the ratio of the attenuated backscatter from unity.

4 Comparison of lidar and ceilometer attenuated backscatter measurements

In this section, an extensive comparison of the simultaneous ceilometer and MUSA observations is reported and discussed. As already mentioned in previous sections, the aerosol backscatter coefficient can be considered to be the only aerosol optical property that can be retrieved using a ceilometer. The first step towards the assessment of the feasibility of backscatter coefficient retrievals using ceilometer observations is the comparison between raw data products provided by co-located ceilometers and advanced lidars.

Unfortunately this is not possible for all ceilometers since signal processing algorithms are often proprietary. Therefore, in the following we compare the attenuated

AMTD
7, 12407–12447, 2014

backscatter available from all the instruments, and different calibration techniques according to the availability of the raw signals. The attenuated backscatter β' is calculated using the Raman lidar retrieval of extinction for the MUSA lidar is defined as (Mona et al., 2009):

$$\beta' = \beta(z) T^2_{\text{par}}(z) T^2_{\text{mol}}(z) T^2_{\text{H}_2\text{O}}(z), \quad (3)$$

$$\beta(z) = \beta_{\text{par}}(z) + \beta_{\text{mol}}(z), \quad (4)$$

where par indicates the contribution of atmospheric particulates, mol is for the molecule contribution and H_2O indicates the water vapor contribution at the operating wavelength. β and T^2 are the backscatter coefficient and the transmittance, respectively. Since in contrast to the 905–910 nm band the 1064 nm wavelength is not significantly influenced by water vapor absorption $T^2_{\text{H}_2\text{O}}(z)$ for MUSA at 1064 nm has been neglected. Wiegner et al. (2014) showed that, if water vapor absorption is excluded, the uncertainty in the retrieved backscatter profile should be lower than 10 %. This accuracy depends on both the ceilometer type and the meteorological condition.

Regarding the retrieval of the attenuated backscatter for each ceilometer, it is calibrated using:

a. the Cloudnet calibration scheme (O'Connor et al., 2004) for the 905–910 nm ceilometer by Vaisala (CT25k);

b. MUSA lidar signals as a reference for the 1064 nm Jenoptik ceilometer (CHM15k) and for the 905–910 nm Campbell ceilometer (CS135s prototype), over an integration time larger than 45 min and using a fixed lidar ratio of 55 sr, obtained from the local climatology of Raman lidar measurements (Mona et al., 2006).

Ceilometer attenuated backscatter profiles have been interpolated at the MUSA altitude levels. Only data above 1200 m a.s.l. have been considered. No overlap corrections have been applied because of the large variability of the overlap correction. To compare 905 and 1064 nm attenuated backscatter profiles, the spectral dependence of

AMTD
7, 12407–12447, 2014

the attenuated backscatter has been considered using an Angstrom coefficient of 1.0 for the aerosol particles, and 905 nm profiles have been scaled accordingly. Errors on the assumption of the Angstrom coefficient are limited to within 1 % (Ansmann et al., 1992).

To provide an overall picture of the performance of the three ceilometers for aerosol layer profiling, we briefly report and discuss a case collected in July 2013. Figure 8 shows a comparison among the simultaneous measurement time series of attenuated backscatter retrieved with CIAO lidar and ceilometers on 11 July 2013 from 20:42 to 22:31 UTC. Since the false color images cannot provide large details of the optically thin layers observed in the free troposphere (visible in the MUSA times series), Fig. 9 shows a comparison among the attenuated backscatter profiles provided by the four instruments on the same day and for the signals integrated from 20:50 to 22:20 UTC. In this plot, all the profiles have been cut at the first point available from the lidar at an altitude of 405 m a.g.l. and the CHM15k is not corrected for the overlap function. The air mass back trajectory (not shown) revealed a continental origin for the observed layers. It is useful to recall that the detection range of the CT25K is limited to 7.5 km a.g.l., the CS135s to 10 km a.g.l. and the CHM15k to 15 km a.g.l. In the presented case, the agreement among the four instruments looks good in the residual layer observed about below 1300 m a.g.l. for the wholes series. Moreover, CHM15k and CS135s are also able to detect the aerosol observed by MUSA in the free troposphere while the CT25k not. It is also important to recall that the CT25K and CS135s are affected by water vapor absorption at their working wavelength (905 nm), where water vapor significantly suppresses laser radiation through absorption.

Comparison of attenuated backscatter

In this section, MUSA and ceilometer attenuated backscatter measurements are compared quantitatively. This is performed by comparing the probability density functions (pdfs) of the β' retrieved for the simultaneous observations performed by the four instruments. In addition, the relationship between the aerosol extinction coefficient (α^{par})

AMTD
7, 12407–12447, 2014

and β' obtained for MUSA is compared with the same relationship obtained for each ceilometer.

Results of this comparison are reported in Fig. 10. Left panels of Fig. 10 show the probability density functions (pdfs) of β' measured by MUSA and each of the ceilometers calculated for the whole INTERACT campaign from 405 to 10 000 m a.g.l. MUSA pdf's are considered as the truth/reference. The number of cases available for each ceilometer and MUSA simultaneously is not the same due to the use of the selection criteria described in Sects. 2 and 3 mainly affecting the CHM15k selected data. This data selection is the reason for the difference among the MUSA pdf reported in the different panels of Fig. 10. Under ideal conditions, the pdf's of the ceilometers and MUSA should be the same. Calibration error and a low SNR can largely affect the comparison. In the case of a calibration error, the pdf could show much higher or much lower values for the ceilometer with respect to the MUSA pdf, though the effect might compensate over the whole dataset. A low SNR, however, can show very high positive and very low negative values affecting, respectively, the values of the pdf higher than the maximum value observed by MUSA and values lower than $1.0 \times 10^{-10}\,\mathrm{m^{-1}\,sr^{-1}}$.

The comparison of the pdfs shows that CHM15k agrees closely with MUSA; CT25K underestimates in a more significant way the values of β' measured by MUSA. CS135s is in very good agreement with MUSA for values lower than $1.7 \times 10^{-6}\,\mathrm{m^{-1}\,sr^{-1}}$, but few larger values of β' are measured by CS135s probably because of the distortion affecting the signal. This indicates that the suppression of the electronic distortion might strongly improve the CS135s performance. Moreover, CT25K shows several very low values of β' ($< 1.0^{-10}\,\mathrm{m^{-1}\,sr^{-1}}$) corresponding to much larger values of β' for MUSA and CHM15k. The other deviations for both the CT25K and CS135s are mainly due their lower SNR than MUSA.

The right panels of Fig. 10 show the same as the left panels but only for the altitude levels above 3000 m. MUSA and CHM15k pdfs show good agreement, though CHM15k overestimates the values of β' below $1.5 \times 10^{-7}\,\mathrm{m^{-1}\,sr^{-1}}$. On the contrary, CS135s tracks MUSA to some extent for the values ranging from $0.5 \times 10^{-7}\,\mathrm{m^{-1}\,sr^{-1}}$ to

AMTD
7, 12407–12447, 2014

$2.4 \times 10^{-7}\,m^{-1}\,sr^{-1}$ but the signal distortion compromises the comparison, and CT25K looks mostly insensitive to aerosol layers above 3000 m a.g.l. This indicates that the CHM15k setup permits better performance over a larger vertical range with respect to CS135s and CT25K which show perform better performance in the boundary layer.

The relationship between the 355 nm aerosol extinction coefficient (α_{355}^{par}) provided by MUSA and the attenuated backscatter β' obtained at 1064 nm by MUSA and by the three ceilometers, respectively, have been compared (Fig. 11) to further investigate the ceilometers' performance and their sensitivity to different aerosol types, i.e. different extinction coefficients,. The parameterα_{355}^{par} is calculated over the same time window as β' but using a lower effective vertical resolution (typically within 480 m) in order to reduce the uncertainty and the related oscillation affecting the extinction profile calculated using the Raman lidar signal. The profile is output at 30 m vertical resolution to match the backscatter vertical resolution. The use of α_{355}^{par} is due to the MUSA measurement configuration which employs an Nd:YAG laser optimized at 355 nm and working with the residual energy at 532 nm; this ensures a higher SNR at 355 nm. Similar results are expected if α_{532}^{par} provided by MUSA is used instead of α_{355}^{par}. In the left panels of Fig. 11, values of β' for the MUSA lidar are reported as a function of α_{355}^{par} obtained by MUSA for each single dataset of simultaneous measurements with each ceilometer; in the right panels, the corresponding values of β' for the three ceilometers are reported as a function of α_{355} obtained by MUSA.

CHM15k shows a very good agreement with MUSA (the regression coefficient of the two attenuated backscatter is $R = 0.95$), though a bit larger dispersion than MUSA in the relationship between α_{355}^{par} and β' is observed. With an increasing value of α_{355}^{par} the difference becomes larger and the value of the β' is overestimated. This is particularly evident for values of α larger than $0.5 \times 10^{-4}\,m^{-1}$. Values of α larger than $0.5 \times 10^{-4}\,m^{-1}$ are mainly located in the atmospheric region below 3 km above the ground.

In the case of the CS135s, three clusters of data are observed: the first corresponds to values of β' higher than $5.0 \times 10^{-7}\,m^{-1}\,sr^{-1}$ and values of α_{355}^{par} lower than

AMTD
7, 12407–12447, 2014

$0.5 \times 10^{-4}\,m^{-1}$ where the values of β' are largely overestimated by the CS135s because of the signal distortion; a second cluster corresponds to values of β' lower than $5.0 \times 10^{-7}\,m^{-1}\,sr^{-1}$ and values of α^{par}_{355} lower than $0.5 \times 10^{-4}\,m^{-1}$, where the relationship looks well estimated but the noise affecting the CS135s is much larger than MUSA; finally, a third cluster corresponds to values of α^{par}_{355} higher than $5.0 \times 10^{-4}\,m^{-1}$, where a small systematic effect seems to increase the values of β' with respect to those measured by MUSA, which is probably related to the effect of environmental temperature, described above, on the CS135s hardware.

Finally, the CT25k show values in good agreement with MUSA for the values of α^{par}_{355} lower than $0.5 \times 10^{-4}\,m^{-1}$. Above this value, in agreement with the analysis reported in Sect. 4.2, a systematic effect appears to increase the values of β' with respect to those measured by MUSA. For values of α^{par}_{355} above $0.5 \times 10^{-4}\,m^{-1}$ the attenuated backscatter values are also strongly affected by an increasing noise due to the decrease of the SNR.

These results demonstrate the existence of limits on the use of ceilometer data in a quantitative way to study aerosol layers, both in the boundary layer and in the free troposphere, with performances that tend to degrade with the increase of both height and aerosol extinction coefficient. A considerable difference between MUSA and the ceilometers is expected and related to large differences in the SNR due to the power of the different laser sources used by an advanced Raman lidar and a ceilometer (see Table 1), though in this study the time resolution of the compared lidar and ceilometer profiles is typically larger than 45 min. Nevertheless, all the plots show a difference between MUSA and ceilometers that looks proportional to the value of β' and α^{par}_{355}, i.e. larger values of β' and α are associated with larger discrepancies between MUSA and each ceilometer. At CIAO, higher values of aerosol optical thickness are typically observed in summer than in fall and winter (Mona et al., 2006; Boselli et al., 2012).,The sensitivity issues ceilometers face in higher aerosol optical thicknesses are compounded by the larger discrepancies between ceilometers and MUSA at higher temperatures and, for the 905 nm instruments, by the higher water vapor content in the

AMTD
7, 12407–12447, 2014

summer. In particular, higher temperatures can decrease the efficiency of the ceilometer hardware and increase the bias of ceilometer attenuated backscatter profiles if calibration is not performed frequently. Other possible reasons for the differences at large values of both of β' and α_{355}^{par} can be related to insufficient dynamic ranges of the systems. Along with the low SNR, this is maybe one of the main reasons for the decreasing performance of CHM15k with increasing range into the free troposphere, shown in Fig. 10. The presence of possible cross cross-talks might further increase the discrepancy though this cannot be evaluated with the considered datasets.

5 Summary and conclusions

The INTERACT campaign carried out at the CIAO observatory in Potenza, South Italy, aimed to evaluate ceilometer aerosol backscatter profiles using the MUSA advanced Raman lidar as a reference. Three commercial ceilometers (CMH15k, CS135s, and CT25K) from different manufactures were deployed and compared with the MUSA lidar, whose stability was also assessed.

The comparisons reveal that, in terms of an overall agreement between each ceilometer and MUSA, the experimental setup of CHM15k has the better performance. However, several limits on the use of ceilometer data in a quantitative way to study aerosol layers are also observed.

The main findings of the investigation are described in the following points.

1. Though they are manufactured in a very robust way and look very rugged, ceilometers are quite sensitive to the large changes in external temperature and collected background levels that occur on daily or seasonal bases; this generates adjustments of system parameters that affect the stability of sensor response over time. It is worth mentioning that this could also be related to problems with the internal temperature sensors of the ceilometers and resulting temperature control or temperature correction errors, though for INTERACT it seems unlikely that this happened for three different systems. Manufacturers should do their best to make

AMTD
7, 12407–12447, 2014

the change of the settings traceable and to quantify the related effects on the signals. Therefore, ceilometer stability over short and mid-term cannot be ensured at the current state of the art, and the use of a forward approach to calibrate a ceilometer using lidar observations or the use of a different calibration method should be frequently re-evaluated and checked.

2. The effect of water vapor on the stability of CC over time has also been evaluated. This effect is non-trivial for ceilometers working at 905–910 nm, while for 1064 nm instruments the effect of water vapor is limited. The correlation between the variability of CC and the variability of the IWV reveals the occurrence of drier conditions in the period when a relevant change of CC is observed for both the CT25K and the CS135s, though water vapor absorption cannot entirely justify the variability of CC observed during INTERACT and it appears to be only one of the effects concurring the variability of CC.

3. Comparison between MUSA and CHM15k exhibits a large instability of the ceilometer in the incomplete overlap region. Though the effect of this on the retrieval of aerosol backscatter can be quantified and is often small, the comparison reveals a large variability in the region from 405 to 890 m a.g.l. while the variability here decreases but still differs within 50 %. Though this is likely to be improved in CHM15kx, this is also a recommendation to avoid the use of an overlap correction function over extended periods of time without regular checks and re-calculation.

4. Differences among MUSA and the ceilometers look proportional to the value of β' and $\alpha_{355}^{\mathrm{par}}$, i.e. larger value of β' and $\alpha_{355}^{\mathrm{par}}$ are associated with larger discrepancies between MUSA and each ceilometer. Larger values of β' and $\alpha_{355}^{\mathrm{par}}$ can be associated with summer and with the increase of surface temperature that affect the stability of ceilometers over short term periods inducing larger discrepancies when the temperature becomes warmer. Moreover, differences at large values of both of β' and α are also probably related to limitations in dynamic range of the systems.

AMTD
7, 12407–12447, 2014

In conclusion, ceilometers show a good potential for aerosol profiling, but they are limited. They have shown promising capabilities in the detection of aerosol plumes in synergy with lidars and/or chemical transport models (Emeis et al., 2011). Though differences among MUSA and the ceilometers are expected by the large difference in the SNR due to the different laser sources used by an advanced lidar and a ceilometer, further technological improvements of ceilometers towards their operational use in the monitoring of the atmospheric aerosol are needed. An extension of the current analysis to daytime is foreseen. Moreover, it has been planned to check historical data from CT25K and CHM15k to confirm or improve the outcome of the INTERACT campaign.

Acknowledgements. The authors are gratefully to Matthias Wiegner for his crucial comments. The financial support for EARLINET by the European Union under grant RICA 025991 in the Sixth Framework Programme is gratefully acknowledged. Since 2011 EARLINET is integrated in the ACTRIS Research Infrastructure Project supported by the European Union Seventh Framework Programme (FP7/2007-2013) under grant agreement no. 262254. The authors would also like to thank Campbell Scientific, Ltd., for contributing the CS135s for this campaign.

References

Ansmann, A., Riebesell, M., and Weitkamp, C.: Measurements of atmospheric aerosol extinction profiles with Raman lidar, Opt. Lett., 15, 746–748, 1990.

Ansmann, A., Wandinger, U., Riebesell, M., Weitkamp, C., and Michaelis, W.: Independent measurement of extinction and backscatter profiles in cirrus clouds by using a combined Raman elastic-backscatter lidar, Appl. Optics, 31, 7113–7131, 1992.

Binietoglou, I., Amodeo, A., D'Amico, G., Giunta, A., Madonna, F., Mona, L., and Pappalardo, G.: Examination of possible synergy between lidar and ceilometer for the monitoring of atmospheric aerosols, in: Lidar Technologies, Techniques, and Measurements for Atmospheric Remote Sensing VII, Proceedings of SPIE Vol. 8182, edited by: Singh, U. N. and Pappalardo, G., SPIE, Bellingham, WA, doi:10.1117/12.897530, 2011.

Boselli, A., Caggiano, R., Cornacchia, C., Madonna, F., Mona, L., Macchiato, M., Pappalardo, G., and Trippetta, S.: Multi year sun-photometer measurements for aerosol

AMTD
7, 12407–12447, 2014

characterization in a Central Mediterranean site, Atmos. Res., 104–105, 98–110, doi:10.1016/j.atmosres.2011.08.002, 2012.
Cimini, D., De Angelis, F., Dupont, J.-C., Pal, S., and Haeffelin, M.: Mixing layer height retrievals by multichannel microwave radiometer observations, Atmos. Meas. Tech., 6, 2941–2951, doi:10.5194/amt-6-2941-2013, 2013.
D'Amico, G., Amodeo, A., Baars, H., Binietoglou, I., Freudenthaler, V., Mattis, I., and Pappalardo, G.: EARLINET single calculus chain – general presentation methodology and strategy, Atmos. Meas. Tech., in preparation, 2014.
Emeis, S., Forkel, R., Junkermann, W., Schäfer, K., Flentje, H., Gilge, S., Fricke, W., Wiegner, M., Freudenthaler, V., Groß, S., Ries, L., Meinhardt, F., Birmili, W., Münkel, C., Obleitner, F., and Suppan, P.: Measurement and simulation of the 16/17 April 2010 Eyjafjallajökull volcanic ash layer dispersion in the northern Alpine region, Atmos. Chem. Phys., 11, 2689–2701, doi:10.5194/acp-11-2689-2011, 2011.
Flentje, H., Claude, H., Elste, T., Gilge, S., Köhler, U., Plass-Dülmer, C., Steinbrecht, W., Thomas, W., Werner, A., and Fricke, W.: The Eyjafjallajökull eruption in April 2010 – detection of volcanic plume using in-situ measurements, ozone sondes and lidar-ceilometer profiles, Atmos. Chem. Phys., 10, 10085–10092, doi:10.5194/acp-10-10085-2010, 2010.
Freudenthaler, V., Esselborn, M., Wiegner, M., Heese, B., Tesche, M., Ansmann, A., Müller, D., Althausen, D., Wirth, M., Fix, A., Ehret, G., Knippertz, P., Toledano, C., Gasteiger, J., Garhammar, M., and Seefeldner, M.: Depolarization ratio profiling at several wavelengths in pure Saharan dust during SAMUM 2006, Tellus B, 61, 165–179, doi:10.1111/j.1600-0889.2008.00396.x, 2009.
Heese, B., Flentje, H., Althausen, D., Ansmann, A., and Frey, S.: Ceilometer lidar comparison: backscatter coefficient retrieval and signal-to-noise ratio determination, Atmos. Meas. Tech., 3, 1763–1770, doi:10.5194/amt-3-1763-2010, 2010.
Illingworth, A. J., Hogan, R. J., O'Connor, E. J., Bouniol, D., Brooks, M. E., Delanoe, J., Donovan, D. P., Gaussiat, N., Goddard, J. W. F., Haeffelin, M., Klein Baltink, H., Krasnov, O. A., Pelon, J., Piriou, J. M., and van Zadelhoff, G. J.: Cloudnet: continuous evaluation of cloud profiles in seven operational models using ground-based observations, B. Am. Meteorol. Soc., 88, 883–898, 2007.
Madonna, F., Amodeo, A., Boselli, A., Cornacchia, C., Cuomo, V., D'Amico, G., Giunta, A., Mona, L., and Pappalardo, G.: CIAO: the CNR-IMAA advanced observatory for atmospheric research, Atmos. Meas. Tech., 4, 1191–1208, doi:10.5194/amt-4-1191-2011, 2011.

AMTD
7, 12407–12447, 2014

Markowicz, K. M., Flatau, P. J., Kardas, A. E., Remiszewska, J., Stelmaszczyk, K., and Woeste, L.: Ceilometer retrieval of the boundary layer vertical aerosol extinction structure, J. Atmos. Ocean. Tech., 25, 928–944, 2008.

Mona, L., Amodeo, A., Pandolfi, M., and Pappalardo, G.: Saharan dust intrusions in the Mediterranean area: three years of Raman lidar measurements, J. Geophys. Res., 111, D16203, doi:10.1029/2005JD006569, 2006.

Mona, L., Pappalardo, G., Amodeo, A., D'Amico, G., Madonna, F., Boselli, A., Giunta, A., Russo, F., and Cuomo, V.: One year of CNR-IMAA multi-wavelength Raman lidar measurements in coincidence with CALIPSO overpasses: Level 1 products comparison, Atmos. Chem. Phys., 9, 7213–7228, doi:10.5194/acp-9-7213-2009, 2009.

O'Connor, E. J., Illingworth, A. J., and Hogan, R. J.: A technique for autocalibration of cloud lidar, J. Atmos. Ocean. Tech., 21, 777–786, 2004.

Pappalardo, G., Amodeo, A., Apituley, A., Comeron, A., Freudenthaler, V., Linné, H., Ansmann, A., Bösenberg, J., D'Amico, G., Mattis, I., Mona, L., Wandinger, U., Amiridis, V., Alados-Arboledas, L., Nicolae, D., and Wiegner, M.: EARLINET: towards an advanced sustainable European aerosol lidar network, Atmos. Meas. Tech., 7, 2389–2409, doi:10.5194/amt-7-2389-2014, 2014.

Stachlewska, I. S., Markowicz, K. M., and Piadlowski, M.: On forward Klett's inversion of ceilometer signals, in: Proc. 25th ILRC International Laser Radar Conference, St. Petersburg, Russia, 5–9 July 2010, 1154–1157, 2010.

Tsaknakis, G., Papayannis, A., Kokkalis, P., Amiridis, V., Kambezidis, H. D., Mamouri, R. E., Georgoussis, G., and Avdikos, G.: Inter-comparison of lidar and ceilometer retrievals for aerosol and Planetary Boundary Layer profiling over Athens, Greece, Atmos. Meas. Tech., 4, 1261–1273, doi:10.5194/amt-4-1261-2011, 2011.

Vande Hey, J.: Design, Implementation, and Characterisation of a Novel Lidar Ceilometer, Ph.D. thesis, Loughborough University, available at: https://dspace.lboro.ac.uk/2134/11853 (last access: 1 October 2014), March 2013.

Vande Hey, J., Coupland, J., Foo, M., Richards, J., and Sandford, A.: Determination of overlap in lidar systems, Appl. Optics, 50, 5791–5797, 2011.

Vande Hey, J., Coupland, J., Richards, J., and Sandford, A.: Design and implementation of a divided-lens lidar ceilometer prototype for manufacture, in: 2012 IEEE International Geoscience and Remote Sensing Symposium (IGARSS), 22–27 July, 5002–5005, 2012.

AMTD
7, 12407–12447, 2014

Wandinger, U., Freudenthaler, V., Baars, H., Amodeo, A., Engelmann, R., Mattis, I., Groß, S., Pappalardo, G., Giunta, A., D'Amico, G., Chaikovsky, A., Osipenko, F., Slesar, A., Nicolae, D., Belegante, L., Talianu, C., Serikov, I., Linné, H., Jansen, F., Apituley, A., Wilson, K., de Graaf, M., Trickl, T., Giehl, H., Adam, M., Comeron, A., Rocadenbosch, F., Sicard, M., Pujadas, M., Molero, F., Alados-Arboledas, L., Preißler, J., Wagner, F., Pereira, S., Lahnor, B., Gausa, M., Grigorev, I., Stoyanov, D., Iarlori, M., and Rizi, V.: EARLINET instrument intercomparison campaigns: overview on strategy and results, Atmos. Meas. Tech. Discuss., in preparation, 2014.

Wiegner, M. and Geiß, A.: Aerosol profiling with the Jenoptik ceilometer CHM15kx, Atmos. Meas. Tech., 5, 1953–1964, doi:10.5194/amt-5-1953-2012, 2012.

Wiegner, M., Gasteiger, J., Groß, S., Schnell, F., Freudenthaler, V., and Forkel, R.: Characterization of the Eyjafjallajökull ash-plume: Potential of lidar remote sensing, Phys. Chem. Earth, 45–46, 79–86, doi:10.1016/j.pce.2011.01.006, 2012.

Wiegner, M., Madonna, F., Binietoglou, I., Forkel, R., Gasteiger, J., Geiß, A., Pappalardo, G., Schäfer, K., and Thomas, W.: What is the benefit of ceilometers for aerosol remote sensing? An answer from EARLINET, Atmos. Meas. Tech., 7, 1979–1997, doi:10.5194/amt-7-1979-2014, 2014.

AMTD
7, 12407–12447, 2014

Table 1. Specification of the MUSA lidar at 1064 nm and of the three intercompared ceilometers. RFOV indicates the half-angle rectangular field of view of the instruments.

Instrument	Wavelength (nm)	Pulse Energy (μJ)	Repetition Rate (kHz)	Configuration	Laser Divergence (mrad)	RFOV (mrad)	Approx. Full Overlap Height (m)
MUSA	1064	5.5×10^5	0.02	Biaxial (0.3° tilt angle between the two axis)	0.10	0.10	330
Jenoptik CHM15k	1064	8	5.0–7.0	Biaxial	0.15 (CHM15k Manual)	0.23 (Wiegner et al., 2014)	1500 (Heese et al., 2010)
Vaisala CT25k	905 ± 5 nm	1.6	5.6	Coaxial common optics	0.75 (CT25k Manual)	0.66 (CT25k Manual)	450–1000*
Campbell Sci CS135s	905 ± 5 nm	3	10.0	Split-lens biaxial	0.35	0.75	300–400 (Vande Hey, 2013)

* Due to the fact that its laser divergence is smaller than its FOV, the CT25k never reaches 100 % overlap. By the convolution calculation method described in Vande Hey et al. (2011), the instrument's optical overlap was calculated for this study from specifications in the CT25k user manual to be: 45 % at 100 m, 78 % at 300 m, 85 % at 500 m, and reaching maximum of 90 % at approximately 1000 m, though unspecified internal corrections which determine the instrument's effective overlap could not be factored into this analysis. Markowicz et al. (2008) reported observing overlap effects of the CT25k directly from its signal to up to 450–550 m.

AMTD
7, 12407–12447, 2014

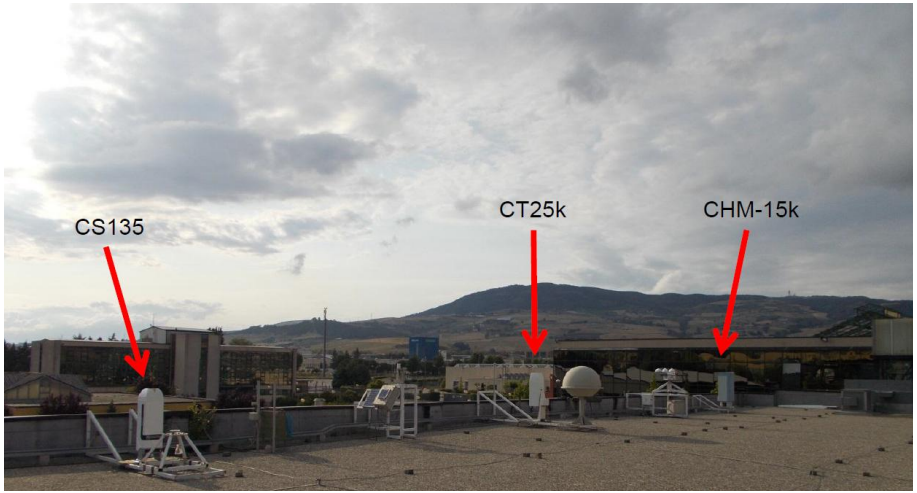

Figure 1. Ceilometer locations on CNR-IMAA Potenza observatory roof.

AMTD
7, 12407–12447, 2014

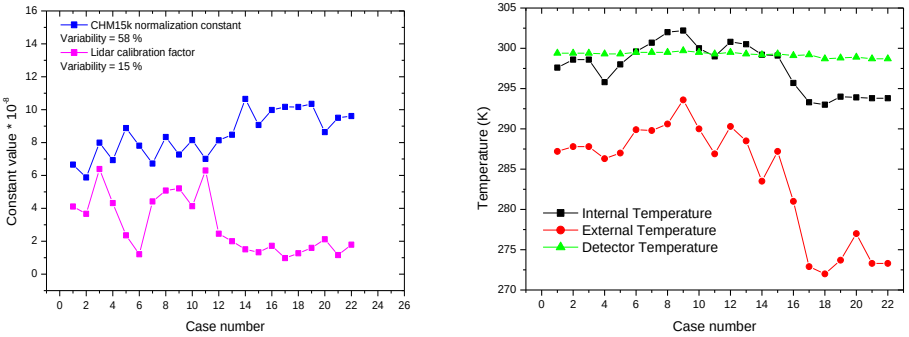

Figure 2. Left panel, the CHM15k calibration constant (blue squares) has been plotted as a function of the case number along with the lidar calibration constant (magenta squares) used for the molecular retrieval of the 1064 nm lidar backscatter coefficient, i.e. the constant used to normalize the lidar 1064 nm profile over the molecular profile; right panel, temperature of the CHM15k detector (green squares), the external (red squares) and the internal temperatures (dark squares) recorded by the instrument sensors for the cases with simultaneous measurements with MUSA.

AMTD
7, 12407–12447, 2014

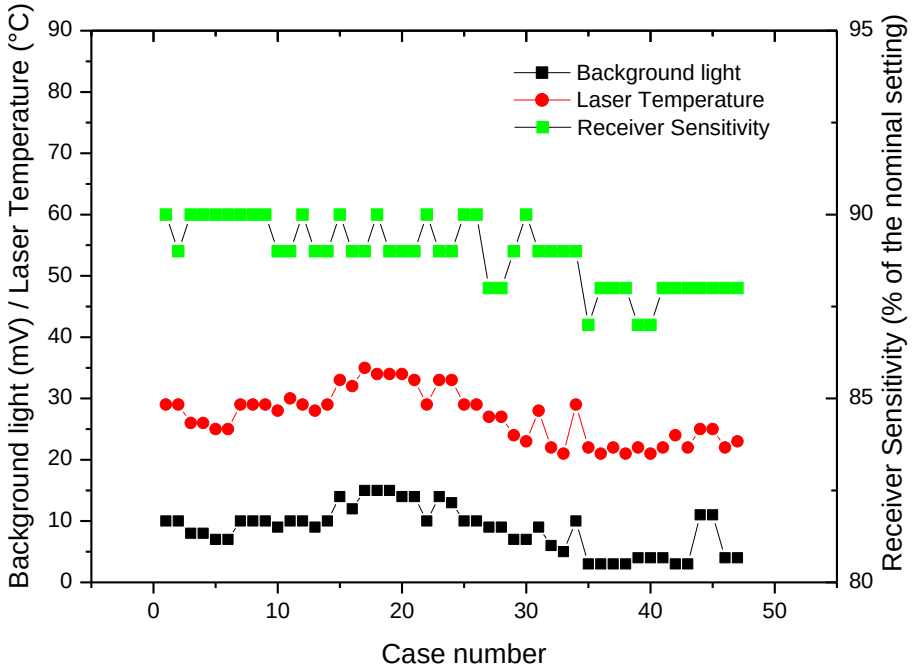

Figure 3. Background light (dark squares), laser temperature (red squares), and receiver sensitivity (green squares) as measured by the internal sensors of the CT25K ceilometer are reported for the cases selected for the comparison with MUSA.

AMTD
7, 12407–12447, 2014

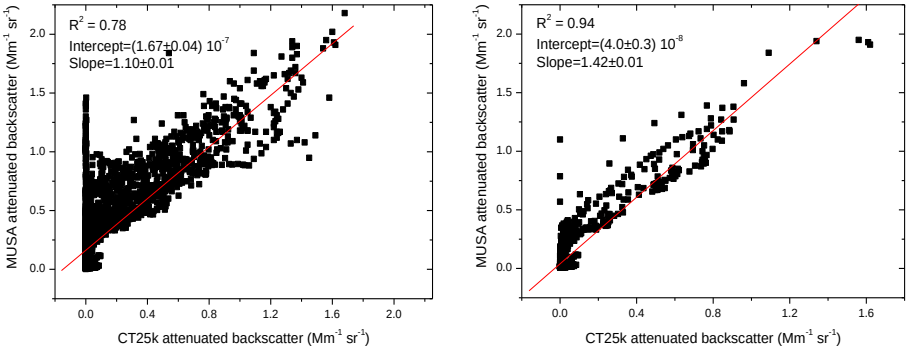

Figure 4. Scatter plot of the attenuated backscatter retrieved by the ceilometer CT25K observations vs. the attenuated backscatter retrieved by MUSA observations; the right panel shows the same plot including only cases from 2 September 2013 onwards when air temperatures were generally cooler.

AMTD
7, 12407–12447, 2014

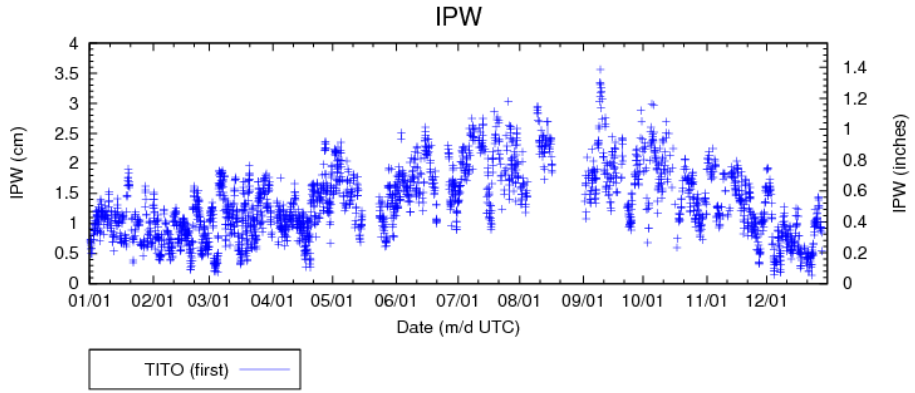

Figure 5. Time series of the integrated water vapour (IWV) content (both in cm and inches) retrieved during the whole year 2013 at CIAO using the GPS technique. The processing of GPS data is provided by NOAA/GSD Ground-Based GPS Meteorology network.

AMTD
7, 12407–12447, 2014

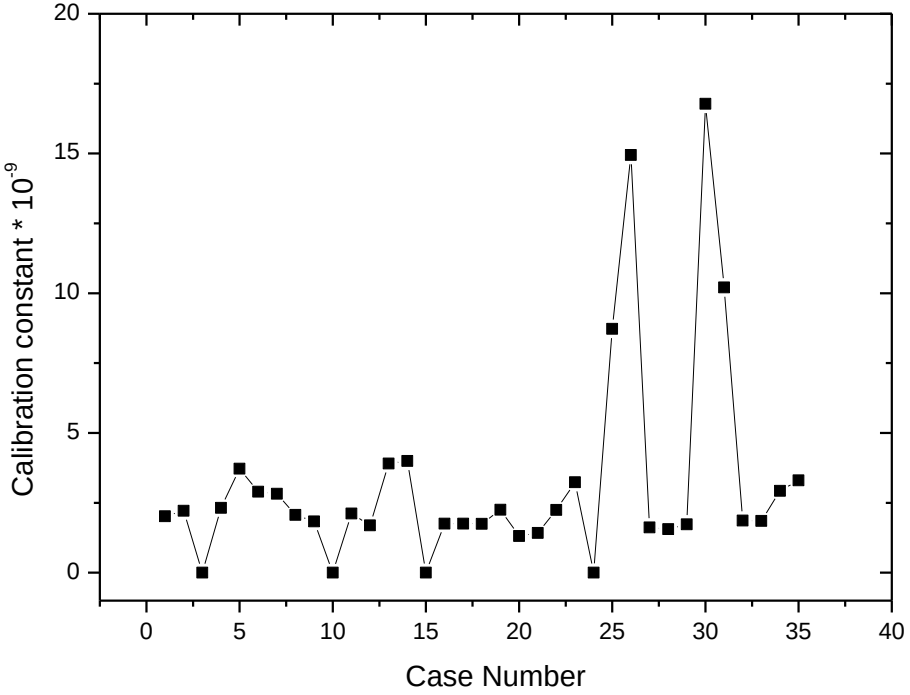

Figure 6. Variability of the calibration constant of the CS135s attenuated backscatter profiles over the corresponding MUSA profiles.

AMTD
7, 12407–12447, 2014

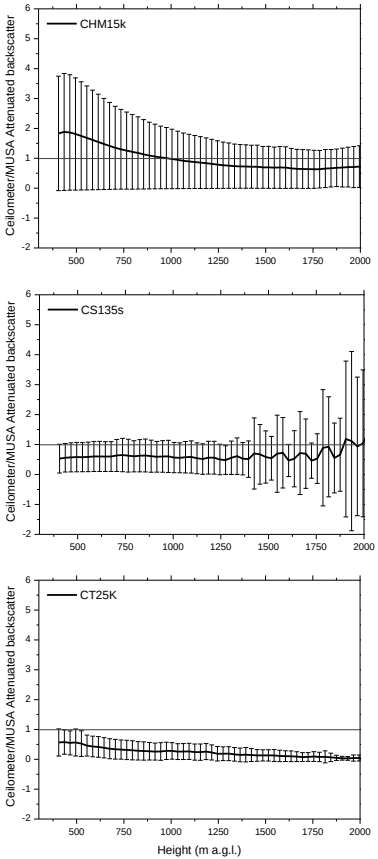

Figure 7. Average (dark line) and SD (vertical bar) of the ratio between the attenuated backscatter measured by each ceilometer and by MUSA. Upper panel is for CHM15k, middle panel for CS135s and lower panel for CT25K.

AMTD
7, 12407–12447, 2014

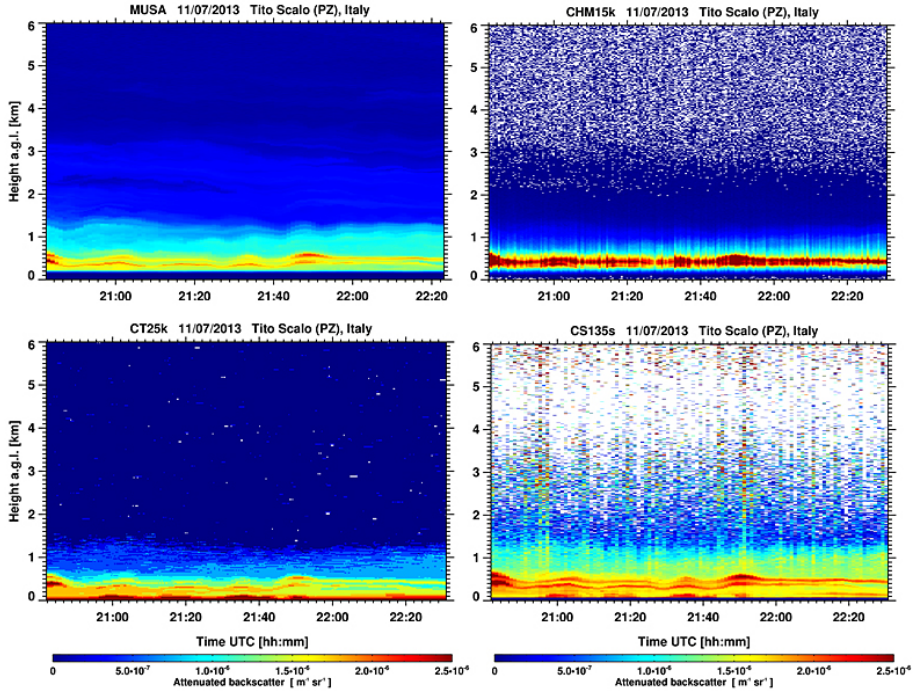

Figure 8. Observation time series of attenuated backscatter collected on 11 July 2013 from 20:42 to 22:31 UTC with MUSA and CHM15k at 1064 nm, and with CT25K and CS135s at 905 nm.

AMTD
7, 12407–12447, 2014

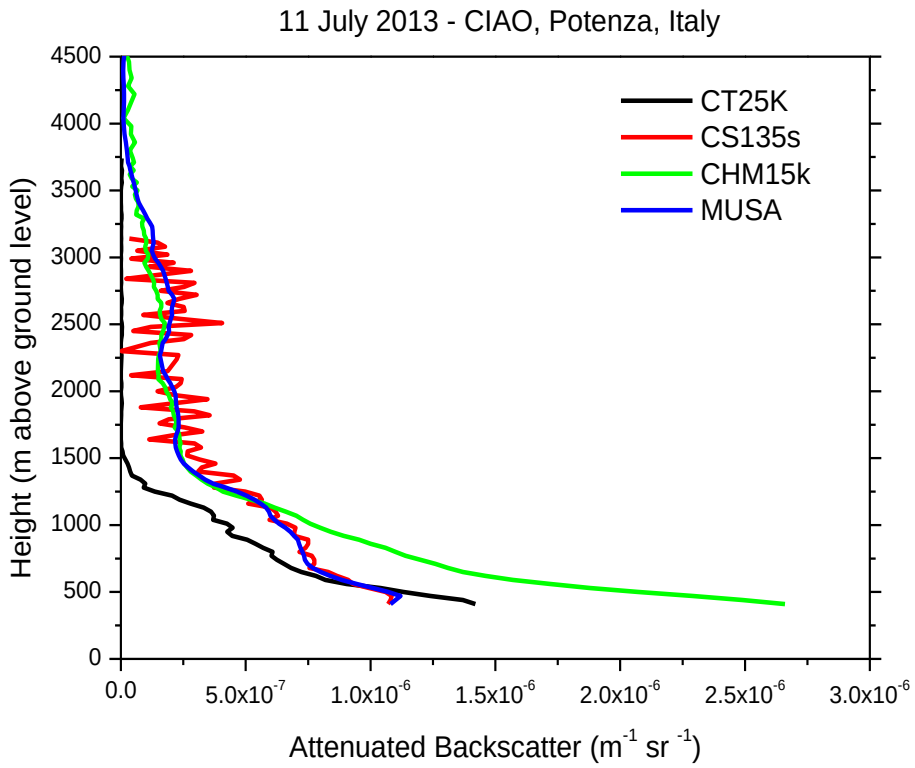

Figure 9. Comparison between the attenuated backscatter profiles provided by the four instruments (MUSA, CHM15k, CT25K, CS135s) on 11 July 2013 from in the time interval between 20:50 and 22:20 UTC. CHM15k is not corrected for the overlap function.

AMTD
7, 12407–12447, 2014

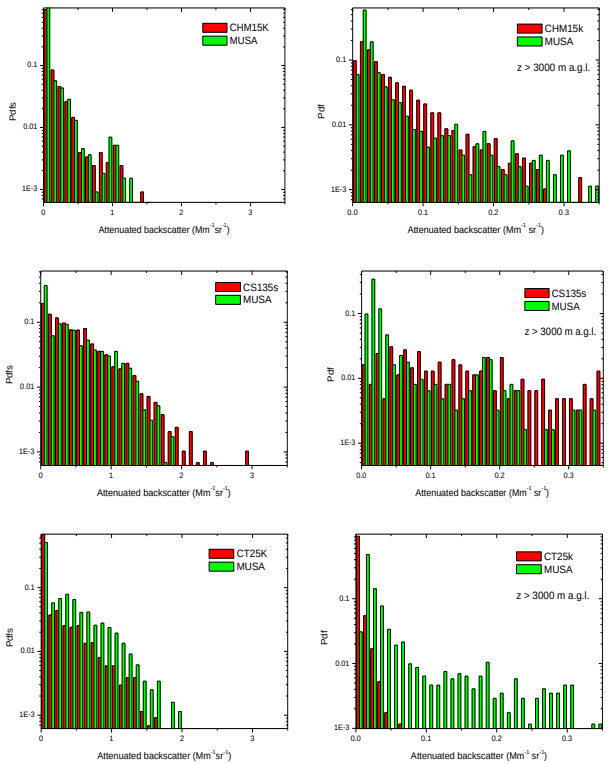

Figure 10. Probability density function of attenuated backscatter values retrieved from simultaneous observations performed by CHM15k and MUSA (upper panels), CS135s and MUSA (middle panels), CT25K and MUSA (lower panels). Left panels include all the values available from each instrument, right panels include only the values measured between above 3000 m a.g.l.

AMTD
7, 12407–12447, 2014

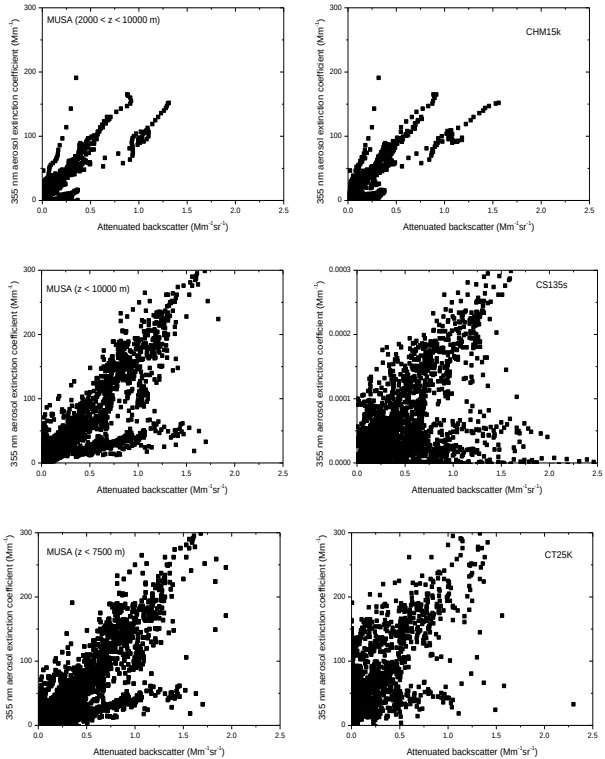

Figure 11. Scatter plot of the attenuated backscatter values retrieved from simultaneous observations performed by MUSA and CHM15k (upper panels), MUSA and CS135s (middle panels), MUSA and CT25K (lower panels) vs. the 355 nm aerosol extinction coefficient obtained from MUSA Raman measurements. The altitude ranges reported on the left plots are due to the incomplete overlap or to the ranging limits of each ceilometer.

AMTD
7, 12407–12447, 2014